Eur Biophys J (2008) 37:111–120
DOI 10.1007/s00249-007-0183-x

ORIGINAL PAPER

Dynamic restacking of *Escherichia Coli* P-pili

Robert A. Lugmaier · Staffan Schedin · Ferdinand Kühner · Martin Benoit

Received: 28 February 2007 / Revised: 27 April 2007 / Accepted: 7 May 2007 / Published online: 7 June 2007

Abstract P-pili of uropathogenic *Escherichia coli* mediate the attachment to epithelial cells in the human urinary tract and kidney and therefore play an important role in infection. A better understanding of this mechanism could help to prevent bacteria from spreading but also provides interesting insights into molecular mechanics for future nanotech applications. The helical rod design of P-pili provides an efficient design to withstand hydrodynamic shear forces. The adhesive PapG unit at the distal end of the P-pilus forms a specific bond with the glycolipid Galabiose. This bond has a potential width $\Delta x = 0.7 \pm 0.15$ nm and a dissociation rate $K_{Off} = 8.0 \cdot 10^{-4} \pm 5.0 \cdot 10^{-4}$ s^{-1}. It withstands a force of ~49 pN under physiological conditions. Additionally, we analyzed the behavior of unstacking and restacking of the P-pilus with dynamic force spectroscopy at velocities between 200 and 7,000 nm/s. Up to a critical extension of 66% of the totally stretched P-pilus, un/restacking was found to be fully reversible at velocities up to 200 nm/s. If the P-pilus is stretched beyond this critical extension a characteristic hysteresis appears upon restacking. This hysteresis originates from a nucleation process comparable to a first-order phase transition in an undercooled liquid. Analysis of the measurement data suggests that 20 PapA monomers are involved in the formation of a nucleation kernel.

R. A. Lugmaier (✉) · F. Kühner · M. Benoit
Lehrstuhl für Angewandte Physik and Center for NanoScience,
Ludwig-Maximilians-Universität München,
Amalienstrasse 54, 80799 Munich, Germany
e-mail: Lugmaier@lmu.de
URL: http://www.biophysik.physik.uni-muenchen.de

S. Schedin
Department of Applied Physics and Electronics,
Umeå University, 90187 Umeå, Sweden

Keywords Atomic force microscope (AFM) · Force spectroscopy · P-pilus · Restacking · *Escherichia Coli* · PapA

Introduction

Latest research shows, that the healthy human body is colonized by up to ten times more external cells i.e. prokaryotes or bacteria, than it consists of somatic cells (Gill et al. 2006). The greater part lives in a symbiotic relation with the eukaryotic organism and therefore provides abilities, from which the human body benefits. This can be the synthesis of amino acids and vitamins out of otherwise indigestible constituents of our nutrition (Gill et al. 2006). *Escherichia coli* cells in the intestinal tract can change from symbiotic to pathogenic if entering the urinary tract. These *E. coli* cells then cause infections (inflammation) and severe pyelonphritis.[1] The extraintestinal infections by *E. coli* often are an underestimated threat causing not only symptoms, which can be cured easily, but also severe diseases with mortality and additionally great economical damage (Russo and Johnson 2003). The understanding of the mechanism of attachment and infection of human epithelial cells by *E. coli* therefore is an important issue for scientists of several subjects.

The P-pili presented in this work are fimbria or hair-like structures expressed on uropathogenic *E. coli* cells, which mediate adhesion to the host tissue. Besides the biological relevance, P-pili show a complex behavior upon stretching and relaxing, which is examined in this work. Its mechanical properties might also be of use as a device in a

[1] Pyelonphritis = upper urinary tract and kidney infection.

future nanoscale ''toolbox'' (Li et al. 2000; Sharma et al. 2006). P-pili are formed by a chaperone-usher pathway in the periplasm of the *E. coli* cell (Bullitt et al. 1996; Sauer et al. 1999, 2002; Vetsch et al. 2004). The P-pili of uropathogenic *E. coli* consist of ca. 1,000 immunoglobulin-like units, so called PapA[2], forming a helical rod (Jiang et al. 2002) (Fig. 1a). At the distal end of the rod resides a tip fibrillum made of one PapK, about 50 PapE units, one PapF and one PapG adhesin which mediates the specific binding to globoseries glycolipids (Galabiose) (Larsson et al. 2003; Lindberg et al. 1984; Lund et al. 1987; Ohlsson et al. 2002) present on human epithelial cells. The P-pilus is anchored to the bacterial cell with a PapH pilin. Except PapG, all Pap-units are quite similar with a molecular mass of about 16,500 Da. The existent strong but non-covalent interactions (hydrogen bonds, hydrophobic interactions) between the subunits n and n + 1 result from ''domain swapping'' (Mu and Bullitt 2006). Thereby the n-terminal β-sheet of the n-th subunit binds into the ''hydrophobic groove'' of the n + 1st subunit. This ''hydrophobic groove'' results from the lack of the seventh c-terminal β-strand of the Ig-like fold (Sauer et al. 2002). In the PapA rod the subunits additionally bind between the n and n + 3rd unit which leads to the rigid helical rod formation (Mu et al. 2005). The right-handed quaternary helical rod has a length of about 1,000 nm and a diameter of 8.2 nm. One turn consists of 3.28 PapA units with an inclination of 2.47 nm (0.754 nm per monomer). The PapA monomer has a molecular weight of 16.5 kDa, a length of 4.1 nm and a diameter of 2.5 nm (Bullitt and Makowski 1998; Mu and Bullitt 2006). Because of the linear alignment of monomers in the tip fibrillum, it has a diameter of 2.5 nm.

To understand the evolutionary developed answers of P-pili to hydrodynamic shear force, mechanical manipulations under well-defined experimental conditions are of great importance. As shown before with Optical Tweezers (OT) experiments, the stretching basically is elastic and therefore reversible (Andersson et al. 2006c). Besides other techniques, the atomic force microscope (AFM) (Binnig et al. 1986; Bippes et al. 2006; Grandbois et al. 1999, 2000) has proven to investigate mechanical properties of living cells (Benoit et al. 1997; Zhang et al. 2006). This work reports on force spectroscopy measurements on P-pili with the AFM. About 70 stretching and relaxing cycles could be measured on one single molecule. The restacking-process of P-pili, present in characteristic force-curves, was the focus of our interest. We discuss the process as a first-order phase transition. Furthermore, with force spectroscopy experiments, we were able to directly measure the failure force of the specific Galabiose-PapG bond. Molecular bonds can be described by the potential of a certain width and depth. According to the Bell-Evans model, the dissociation rate increases with the potential width Δx and with an applied force F(t) (Evans and Ritchie 1997, 1999). Based on this theory and the characteristic distribution of the measured failure forces we will determine the natural dissociation rate K_{off} and the potential width Δx for the PapG-Galabiose bond by a Monte Carlo simulation (Friedsam et al. 2003). A unique feature in this work is the combination of the AFM with a high-resolution light microscopy technique that allows us to select very precisely an individual bacterial cell for the force spectroscopy measurement (Fig. 1b).

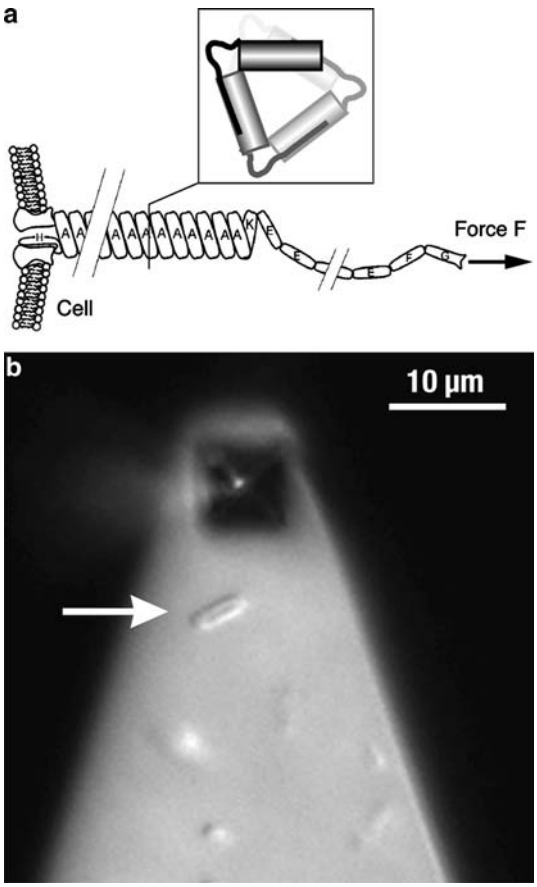

Fig. 1 **a** Structure of an *E.coli* P-pilus [derived from Jass et al. (2004)]. The P-pilus consists of ca. 1,000 PapA units forming a helical rod with a length of about 1,000 nm and a diameter of 8.2 nm. At the distal end resides a non-stacked tip fibrillum consisting of one PapK, ca. 50 PapE, one PapF and one PapG protein. The PapG protein specifically recognizes the gylcolipid Galabiose present on human epithelial cells. *Inset* Cross section (derived from Mu and Bullitt (2006)). The units are connected via ''domain swapping''. **b** Quasi-Trans DIC image of *E. coli* cells on a glass substrate positioned below the reflecting AFM-cantilever (unsharp edges because out of focus). Quasi-Trans DIC microscopy allows high-resolution optical imaging below a reflective surface (here the cantilever). The cell (*arrow*) and the very top of the pyramidal tip are in focus. For the measurements the single cell was translocated to directly get into contact with the cantilever tip

[2] Pap = Protein associated with pyelonphritis.

Materials and methods

Substrate- and cantilever-functionalization

The Si_3N_4 AFM-cantilevers (MLCT-AUHW, Veeco Inc., Santa Barbara, CA, USA) were thoroughly cleaned in ethanol and dried at 80°C. They were incubated in pure aminosilane (N^1-[3-(Trimethoxisilyl)-propyl-diethylenetriamine], Sigma-Aldrich Chemie GmbH, Munich, Germany) at 80°C for 10 min, rinsed with ethanol and baked in water at 80°C for 1 h. Then carboxymethylamylose (CMA, Sigma-Aldrich) was covalently bound to the aminosilane via EDC/NHS (1-ethyl-3-[3-(dimethylamino)propyl]carbamide/N-Hydroxysuccinimide, Sigma-Aldrich) activation. For the studies of the specific receptor-ligand interaction of PapG to Galabiose, Amino-Galabiose (2 mM, $C_{14}H_{27}NO_{11}$) (Ohlsson et al. 2002) was covalently coupled to the activated CMA on the cantilever. For the restacking experiments the activated CMA cantilever was directly used to bind to a pilus.

To make full use of the optical resolution of the AFM-Hybrid (see below), the measurements were performed in homemade glass-bottom Petri dishes. Round cover glasses (Carl Roth GmbH & Co. KG, Karlsruhe, Germany) with a thickness of 0.17 mm were silanized and functionalized with CMA as described for the cantilevers. After drying the cover glasses in a nitrogen flow, they were glued onto a hole punched into a commercially available plastic Petri dish (Nunc, Roskilde, Denmark).

Bacteria and culture conditions

P-pili were expressed in recombinant derivatives of the otherwise afimbriated *E. coli* HB101.

The plasmid pPAP5 carries the entire Pap gene cluster on the vector pBR322 and expresses normal P-pili. The pPAN5 carries a mutant Pap gene cluster which expresses fewer PapA subunits and therefore shorter P-pili (Lindberg et al. 1984). The HB101/pPAP5 *E. coli* bacteria were cultured on tryptic soy agar (TSA, Sigma-Aldrich), supplemented with 50 µg/ml carbenicillin (Sigma-Aldrich). Shortly before the AFM measurements the cells were resuspended in phosphate buffered saline, pH 7.4 (PBS, Sigma-Aldrich).

AFM experiments

The force spectroscopy experiments were performed with an AFM-optical microscope hybrid-instrument described in Lugmaier et al. (2005). This instrument consists of a 1D-AFM head placed on top of an inverted microscope. With a magnification up to the Abbe diffraction limit and high vibration damping, this setup combines high-resolution optical microscopy and high-resolution force spectroscopy.

A droplet (40 µl) of suspended cells was put on the EDC/NHS re-activated cover glass. The cells were allowed to settle for 30 min and to bind covalently via their amino-groups to the Carboxymethylamylose. After rinsing carefully, we added fresh PBS buffer for the measurements. After the preparation the cells were used for about 2 h. With the use of the Quasi-Trans DIC technique (Lugmaier et al. 2005) and an exactly tunable x-y-stage we were able to place a single *E. coli* cell directly under the tip of the AFM-cantilever (see Fig. 1b). After this alignment, the cantilever was brought into contact with the cell at contact forces lower than 100 pN and a contact time of 3 s to allow the pili to bind. Galabiose-functionalized cantilevers were used to record the interaction with PapG located at the very end of each pilus. Force-distance curves were recorded at 500 nm/s. In control experiments this interaction was blocked by adding 2 mM soluble Galabiose ($C_{19}H_{28}O_{12}$). For the dynamical restacking experiments force-distance curves were recorded at velocities in the range between 200 and 7,000 nm/s. The elongation of pili of different lengths was modulated at varied extensions. With the Igor Pro Software (Wavemetrics Inc., Lake Oswego, Oregon, USA) the curves were recorded (20 kHz sampling frequency; 10 kHz filtering) and analyzed (smoothed force curves: box-smoothing, box size 51).

Monte Carlo simulation

The bound state of a receptor ligand interaction can be described using a potential well, which can be left with a certain probability. This unbinding process is driven by thermal fluctuations. According to the Bell–Evans model, mechanical loading of the bond deforms the energy landscape. Hence, the probability for dissociation under an applied force $F(t)$ depends on the natural dissociation rate K_{off} but also on the potential width Δx (Evans and Ritchie 1997, 1999):

$$K_{\text{off}}(F) = K_{\text{off}} \cdot \exp(F \cdot \Delta x / k_{\text{B}} \cdot \text{T}).$$

The thermal fluctuations lead to a characteristic distribution of the measured failure force F of every molecular bond if this bond is loaded with force by the AFM cantilever at a certain retraction velocity v. The Monte Carlo simulation computes the dissociation probability $P(F) = K_{\text{off}}(F) \cdot \Delta t$ (with $\Delta t = \Delta z/v$ = sampling interval divided by the separation velocity) (Rief et al. 1997a). A master force curve was constructed, which exactly reproduces the force profile when stretching a pilus (compare Fig. 2a). To consider the different pili lengths, the unbinding events are weighted according to their occurrence in the experiment to scale a

representative master curve. The simulation is performed by calculating the dissociation probability $P(F)$ for every point (interval Δz) on the force profile. Δt is the time scale of the applied force F. $P(F)$ is compared with a random number between zero and one. If $P(F)$ is larger than this random number, the corresponding force equals the unbinding force and the next run starts. For further details see the introduction of this method in Friedsam et al. (2003). The obtained distribution is plotted together with the histogram of the measured rupture forces, which is a summation over three experiments (Fig. 4b). By varying the intrinsic values K_{off} and Δx, the dissociation probability function $P(F)$ is fitted to the rupture force histogram. This method is applied to the measured data recorded at a single retract velocity and not only considers the maxima of the histograms but also its shape.

Experimental results

Unstacking and restacking dynamics

Figure 2a shows a typical force versus extension curve of a single P-pilus. The *E.coli* cell that expresses the pilus was bound to a carboxylated surface. The pilus is picked up unspecifically with the AFM-cantilever and can be stretched up to fivefold of its length until rupture or detachment. One can easily distinguish three major regions (compare Jass et al. (2004)): Region I refers to the first rise (sometimes with a starting peak) where the first unstacking of the PapA units occurs. Region II shows a further unstacking of the helical rod, which leads to a constant force plateau at about 27 pN. Finally region III shows a second plateau and a drastic increase of the force due to an elastic stretching of the pilus (i.e. a molecular chain). The particular shape of the force curve throughout regions I-III and the constant level of ~27 pN at the plateau in region II provide a unique ''fingerprint'' that is used to distinguish single pili attachments from multiple bonds. By stopping the cantilever movement before a rupture event and by subsequently decreasing the tip–surface distance, the pilus is able to restack by reorganizing its helically stacked structure. The typical trace shown in Fig. 2b shows that the restacking is exactly the same as the unstacking path, except for the hysteresis which occurs before re-entering the constant force plateau in region II (in a few cases additional areas with hysteresis occur, see below). At the hysteresis region in the relaxation curve the tension in the pilus is reduced down to 17 pN. Next, a steep increase in force up to the first plateau marks the end of the hysteresis. It seems that a restacking seed had to be formed. Further relaxation exactly follows the former unstacking plateau

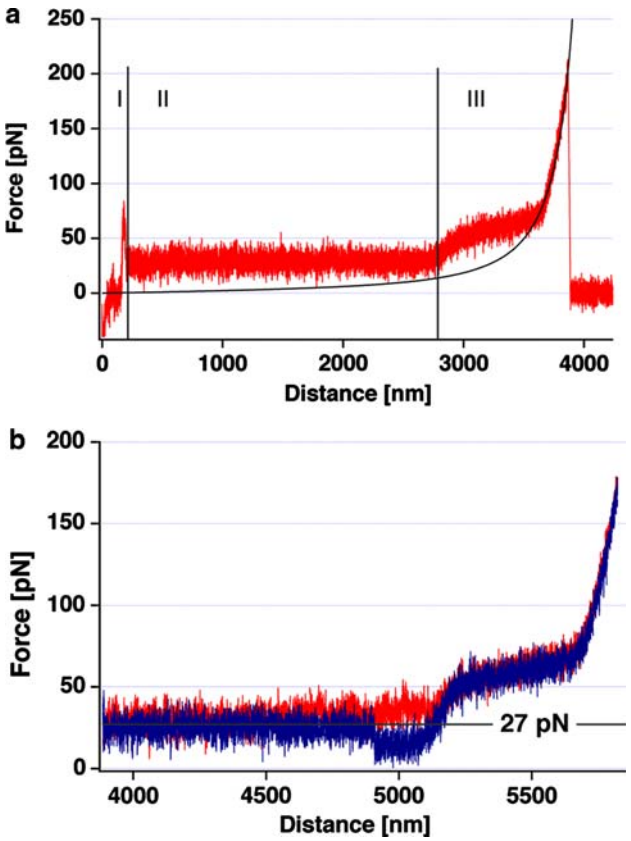

Fig. 2 **a** Force versus elongation plot of one single pilus, adhering nonspecifically to the tip, measured at a velocity of 500 nm/s. Region I (initial unstacking), II (unstacking plateau at a force of 27 pN) and III (further stretching until the rupture event occurs) are indicated in the figure. *Black Curve* WLC fit to the final elongation (Persistence length L_p = 0.78 nm, Contour length L_c = 4212 nm). **b** Force versus elongation plot of one single pilus ranging from region II into region III (*red*). The relaxation curve (*blue*) shows the characteristic hysteresis. The measurement was performed at a velocity of 500 nm/s

at the same equilibrium force of 27 pN. This un-/restacking force curve can be reproduced repeatedly until the pilus finally separates from the tip. This final separation curve reveals whether it was a single-pilus experiment. If other pili would remain connected to the tip, the first force-plateau would show additional steps to multiples of 27 pN.

Figure 3 shows a set of 70 restacking curves of one and the same single pilus at eight different velocities between 200 and 7,000 nm/s. Curves recorded at the same velocities are pooled. To obtain these curves, the pilus was bound unspecifically to the tip of the AFM cantilever. This attachment holds forces up to 250 pN and therefore allows the recording of several stretching and relaxing cycles without detachment of the pilus. We define the length l of the hysteresis (according to Fig. 3) between the reference point P (red circle) and the beginning of the abrupt rise to the restacking plateau. At the velocity of 200 nm/s, P is the

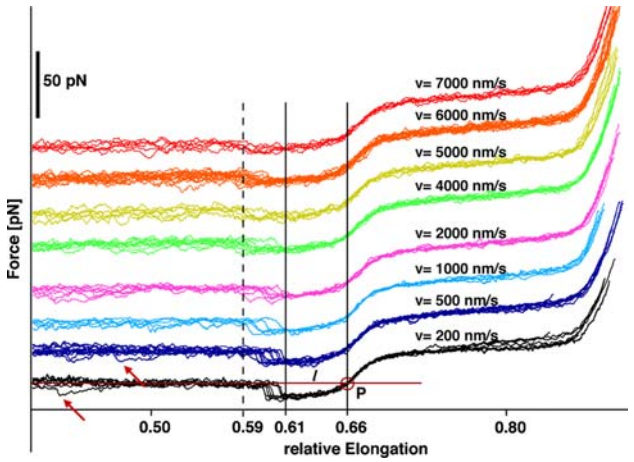

Fig. 3 Velocity dependent force curves of one single pilus. Restacking is limited by a spatial barrier, which leads to a minimum hysteresis length of 270 nm. The X-axis shows the relative elongation of the pilus with respect to its contour length L_c (see WLC fit in Fig. 2a). Longest restacking-events occur at 0.59 L_c (*dashed y-line*), shortest at 0.61·L_c (*solid y-line*). *P* marked by a *red circle*, represents the intersection of the line-fit of the plateau with the decreasing part of the restacking curve and is equivalent to the critical elongation point. This fixed point *P* is located at 0.66 L_c (*solid y-line*). The value ''*l*'' indicates the length of the hysteresis, measured from P to each restacking step. *Arrows* indicate drops within the restacking plateau with a similar shape like the hysteresis plateaus

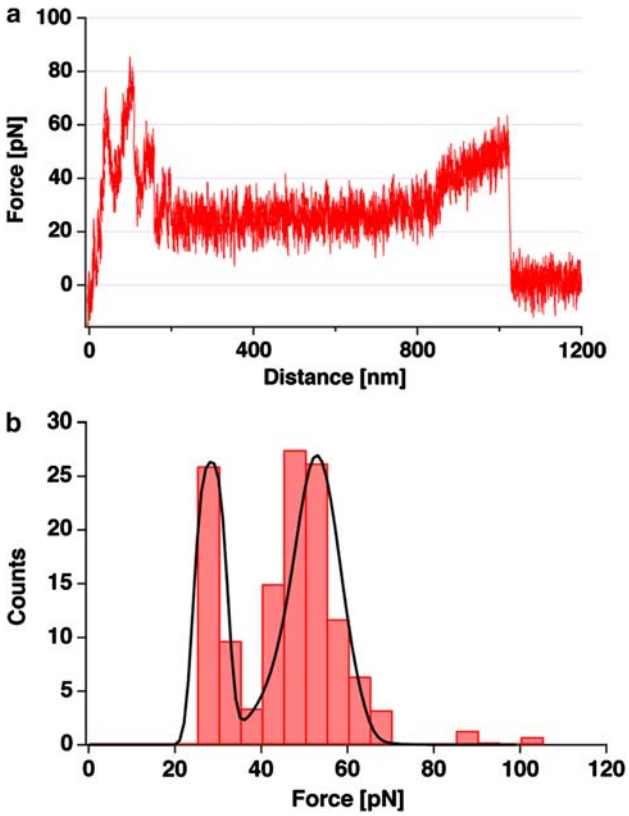

Fig. 4 **a** Typical force–distance plot of the opening of a Galabiose–PapG bond (here 44 pN). **b** Force histogram of all measured rupture events of Galabiose–PapG bonds. The histogram reveals most probable rupture forces of 27 and 49 ± 3 pN. By varying the intrinsic values K_{off} and Δx, the dissociation probability function P(F) can be adjusted to equal the measured rupture force histogram. The *black solid line* shows the best Monte Carlo fit with a dissociation rate $K_{Off} = 8.0 \cdot 10^{-4} \pm 5.0 \cdot 10^{-4}$ s^{-1} and a potential width Δx = 0.7 ± 0.15 nm

intersection of the line fit to the plateau with the steep force slope between the hysteresis and the second plateau. Interestingly, our measurements show, that this point P marks another decisive behavior: If stretching of the pilus is reversed before passing this ''critical extension'' of 66% of the total contour-length (point P), the restacking precisely follows the unstacking pathway without showing any hysteresis. In contrast, if the pilus is stretched beyond this point P, the hysteresis appears in the relaxing force curve. Furthermore, we found that the shape of the region to the right of the reference point P is conserved even under different velocities for all curves [compare Andersson et al. (2006b)]. In Fig. 3 the curves are aligned in the x-direction at the point P. The curves recorded at 200 nm/s thereby serve as template for the alignment. This alignment assures the measure of the hysteresis length *l* independent of hydrodynamic effects of the cantilever. Moreover, when relaxing the pilus at higher cantilever speeds the constant force plateau is lowered due to limited restacking kinetics (see Discussion).

An analysis of the hysteresis length *l* shows, that it ends in the range of 59–61% of the contour length L_c for all velocities (Fig. 3). The refolding step is flattened at higher velocities but the hysteresis is still recognizable after computer processing of the data (noise filtering and compressing the curve in x-direction). The slope of the step at the end of the hysteresis up to the stacking plateau varies with different cantilever velocities. Through normalization with respect to time, one obtains a constant value for the ''speed for the initiation of restacking'' of 18 ± 1 nm/s for all recorded curves.

Specific PapG-Galabiose bond

Figure 4a shows a typical force-curve with a specific interaction between Galabiose and PapG. The detachment forces obtained from three experiments are shown in the histogram in Fig. 4b and reveal a bimodal distribution with peaks at 27 and 49 ± 3 pN, which refer to the most probable rupture forces. The adhesion dropped below the detection limit if soluble Galabiose was added, which corroborates the specificity of this interaction. A probability dissociation function can be computed by a Monte Carlo simulation (Evans and Ritchie 1997, 1999) (see Materials and methods). Fitting this function to the experimental results, by varying the intrinsic values K_{Off}

and Δx (black solid line in Fig. 4b) yielded a dissociation rate $K_{Off} = 8.0 \cdot 10^{-4} \pm 5.0 \cdot 10^{-4}$ s^{-1} and a potential width $\Delta x = 0.7 \pm 0.15$ nm for the PapG-Galabiose complex.

Theory

Model for dynamic restacking

In agreement with other models we assume that the pilus is partially stacked with an angle of 13° between the subsequent units (Bullitt and Makowski 1995; Mu and Bullitt 2006). A nucleation force (region I at the beginning of the elongation force curve, Fig. 2a) is needed to first break up the stacking of the PapA units somewhere in the pilus. Now the PapA units can subsequently unstack at an equilibrium force of 27 ± 3 pN in a process, which can be discussed in analogy to a phase transition. It is assumed, that the unstacking force results from the opening of the bond between the n-th and the n + 3rd subunit (Andersson et al. 2006a). This force tends to pull the PapA units back into the stacked conformation in equilibrium with a force stretching the angle between the unstacked units. Andersson et al. (2006a) suggest a ''strain-assisted bond-opening'' for the pilus elongation in their modified ''sticky chain'' model (Jager 2001). At the critical extension of 66% all the stacked units are opened and the force increases to the second plateau where the units are forced to overcome a steric hindrance by deforming their tertiary structure (Thomas et al. 2002). This deformation must be faster than the unstacking process, because it does not show any structural hysteresis even at high velocities as 2 μm/s (except hydrodynamics of the cantilever). On further stretching of the pilus (the angles between the units become close to 180°) the typical pattern of a worm like chain (Rief et al. 1997b) fits to the slope until the rupture event occurs (Fig. 2a).

The nucleation process required to initiate restacking

We assume that a nucleation process triggers the steep step at the end of the hysteresis upon relaxing the pilus. This step establishes the initial stacking of PapA units and requires a relaxation to at least 0.61 contour length L_c (Fig. 3). The latest steps towards restacking occur at a length of 0.59 L_c of the relaxing pilus (when taking into account all the curves of the complete set of velocities). As soon as this stacking is established it obviously stabilizes an equilibrium force between the units, which equals the unstacking force of the plateau and might act as a seed for the unstacked units to join the stacking. Comparable to undercooled liquids, formation of a nucleation kernel of critical size (indepent of the liquids volume) initiates first-order phase transitions. In analogy to this, a nucleation kernel for restacking might be detected by comparing pili of different lengths. Therefore, we compare relaxation curves of pili of different lengths by scaling them to a normalized length. To obtain the most precise results we took only measurements at the same velocity of 200 nm/s into account since the variation in hysteresis length is smallest at this velocity (see Fig. 3). An arbitrary pilus restacking force curve was defined as a reference for a standard pilus length (e.g. black curve in Fig. 5). Each curve from pili with different lengths can be scaled to this standard by an individual scaling factor k in order to superimpose the conserved part. This conserved part spans from the maximum extension through the second plateau down to the beginning of the restacking hysteresis at the reference point P. Its length L was used to determine the scaling factor $k = L_0/L$, where L_o is the conserved length of the reference standard pilus. This classification is reasonable, since already in Fig. 3 the conserved part could be identified, while the length of the hysteresis plateau varies. As expected for a pilus trying to restack like in a situation comparable to an undercooled liquid, the initial step to start restacking is very sensitive to the statistical kicks due to the Brownian Motion. Therefore, the hysteresis lengths l do not superimpose exactly, as shown in Fig. 3 even within the same pilus. But interestingly the average of the longer pili exhibits shorter hysteresis l' after the scaling and vice versa (see Fig. 5). A reason for this could be an unknown structure of a length a_o in each restacking hysteresis, which is constant and independent of the pilis' lengths. On this basis we define the plateau length of the hysteresis for the standard pilus as:

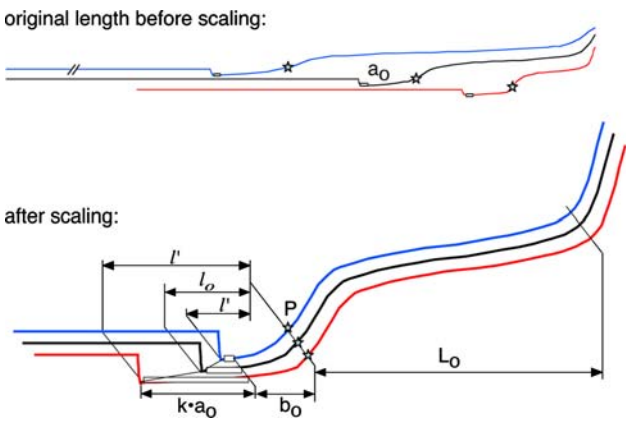

Fig. 5 Scaling model and calculation. Before scaling: Pili with different lengths but equal nucleation kernel a_0. Standard pilus (*black*), short pilus (*red*), long pilus (*blue*), critical elongation point (*star*). After scaling: Pili have the same conservative length L_0 and b_0 but $k \cdot a_0$ changes according to the scaling: for short pili to a longer hysteresis l' (*red*) and for long pili vice versa (*blue*)

$l_0 = a_0 + b_0$.

Analogous the plateau length of any other pilus refers to:

$l = a_0 + b$.

By scaling from L to L_o ($L_o = k{\cdot}L$) b scales to b_o ($b_o = k{\cdot}b$). But a_o does not scale. Therefore, the scaled plateau length l' refers to:

$$l' = k{\cdot}l = k{\cdot}a_0 + k{\cdot}b = k{\cdot}a_0 + b_0$$

by replacing b_o with $l_o = a_o + b_o$;

$$b_0 = l_0 - a_0;$$

$$l' = k{\cdot}a_0 + l_0 - a_0 = l_0 + a_0{\cdot}(k-1).$$

In order to obtain a value for a_o we plotted the scaled length of the restacking hysteresis versus the original length of this hysteresis and fitted the data with the equation $l' = l_o + a_o \cdot (k - 1)$. With a_o as the only fit parameter we retrieve a value of 47 ± 17 nm for a_o. The fit is shown in Fig. 6 where additionally the nucleation length $a_o{\cdot}k$ is subtracted from the hysteresis length $l{\cdot}k$. This shows, that without the constant length a_o each pilus would superimpose after scaling within the thermal driven variation of the hysteresis length. The length a_o will be interpreted as a nucleation length, which is required for the occurrence of stacking and is related to geometrical factors of the unstacked pilus.

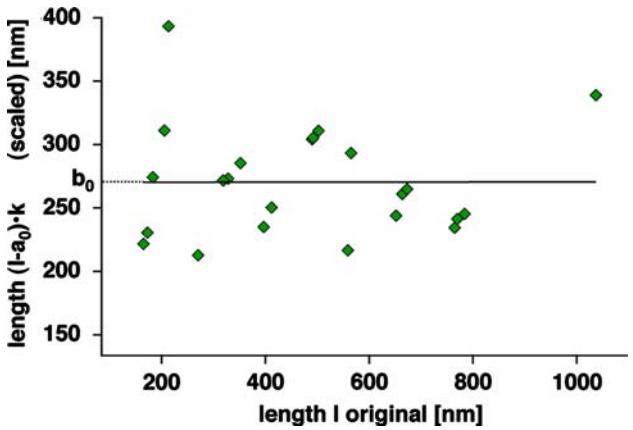

Fig. 6 Length of the hystersis $l{\cdot}k$ after scaling minus the nucleation length $a_0{\cdot}k$ plotted versus the original (unscaled) hysteresis length. After subtracting a_0 from each pilus, the black line-fit to the scaled remaining hysteresis length b_0 shows that the pilus now scales over its complete length. That means that the nucleation length a_0 is independent of the pilus length, whereas $b_0 = l_0 - a_0$ is the part of the hysteresis, which depends on it. The variance of the hysteresis length distribution is due to the influence of the thermal energy

Discussion

Nucleation seed formation

Relaxation of the pilus below an extension of 61% of the contour length L_c allows the formation of a nucleation seed, which is sufficient for restacking. Apart from the tip fibrillum and the membrane anchor PapH, the pilus is homogeneously composed of identical PapA units. A singular domain of the pilus, like the tip fibrillum, is conceivable to induce the nucleation. But since the pilus is grabbed non-specifically on any Pap unit, it is improbable that these structures significantly contribute to the stacking. Furthermore, the hysteresis pattern is not a singular event while restacking: in some force curves additional hysteresis-like patterns can be observed during the restacking within the first plateau (see the arrows to the lower left in Fig. 3). We interpret this as additional nucleation seeds due to stuck restacking. For these reasons neither the single PapH nor the tip fibrillum with an estimated length of roughly 200 nm seems to originate the nucleation seeds for stacking nor to contribute for the scaling mismatch a_o.

In our picture, the stacking only is possible after a certain number of PapA units had formed a spontaneous nucleation seed. When transforming the nucleation length a_o into a number of PapA units at the actual pilus extension of 61% L_c we obtain 20 ± 7 PapA units or five turns (47 nm/(4.1 nm·0.61)). Calculating the hysteresis area, which corresponds to the length of 47 nm of the nucleation kernel, one can estimate a nucleation energy of about 4.8 k_BT per kernel unit[3] needed for restacking.

Dynamic restacking

Our results from the dynamic measurements are in good agreement with those from existing OT experiments. The fact that especially in OT experiments additional hysteresis-like patterns (drops) occur while restacking within the first plateau indicates, that the torque in the pilus also has an influence on the polymerisation of the stacked region. These additional spontaneous drops occur in almost every OT force curve when relaxing within the first plateau (Andersson et al. 2006c). They are rare in AFM experiments (below 10%) as indicated with the arrows in Fig. 3. A possible explanation for this could be the different boundary conditions in an AFM and an OT experiment. In an OT experiment, the trapped spherical bead in the laser-focus, to which a single pilus is bound, can freely rotate around the axis of the pilus. That is, the pilus is allowed to relax its torsion by rotating the bead in the laser-focus

[3] (length of nucleation kernel × force difference to the plateau)/(# PapA·4.1 pNnm) = (47 nm·8.3 pN)/(20·4.1 pNnm) = 4.8 k_BT.

during the experiment. The torsion has to be regained if the pilus wants to restack into the helical rod formation upon relaxation. In contrast, the pilus is fixed between the cantilever tip and the anchorage of the *E. coli* membrane in an AFM experiment. This might preserve torsion and ease the restacking.

In both, the OT and the AFM measurements we have a certain decrease of the height in the constant force plateau while restacking with an increased velocity and the unstacking occurs at higher forces. After subtracting the additional force caused by cantilever hydrodynamics (8.68 ± 0.11 pN s/μm) (Janovjak et al. 2005), still a force offset between expansion and retraction remains. This lowering of the restacking force plateau with increasing speed is the same as in the OT experiments (Fig. 3). It is due to the finite restacking kinetics required for the bond ruptures and formations respectively (Andersson et al. 2006b). As shown above, the initial formation of the restacking seed takes place at a velocity of only 18 nm/s. Nevertheless the restacking plateau is not lowered yet to zero even at velocities of 7 μm/s. The 2nd Plateau (region III) is passed through in thermal equilibrium fully reversible for all measured velocities. This indicates that the kinetics of the pilus transformations in this region is much faster than 7 μm/s. The forces suggest entropic stretching as well as pure elastic deformations in the molecular structure. For the restacking plateau (region II) the equilibrium condition (unstacking curve identically reproduces the restacking curve) only holds for velocities at 200 nm/s and below (data not shown). Of course, the hysteresis itself is not an equilibrium process. Nevertheless it should be mentioned, that the relaxing part (lower part) of the hysteresis is highly conserved at all measured velocities. This again indicates fast kinetics originated from entropic and elastic deformations of the PapA units.

The hysteresis in the relaxing force curve represents the unstacked PapA units in a metastable phase comparable to an undercooled liquid (Spinella et al. 1998). This state starts from the binodial point (reference point P). Upon further relaxing, the probability for cooperative fluctuations and therefore for nucleation seed formation increases. Nucleation seeds need to reach a critical size to start phase transition. For restacking, we determined a possible kernel size to be 20 ± 7 PapA units. We measured mechanical nucleation energy of 4.8 ± 1.7 k_BT per seed unit. This nucleation earliest occurs at 61% elongation for all velocities. For high velocities, the latest seed formation is shifted to lower elongations until the spinodial point is reached at 59% (see Fig. 3). Then the phase transition takes place while the two phases of stacked and unstacked PapA units coexist in a stable equilibrium at 27 pN. Seed formation is an important but not trivial process and will be topic of further investigations.

Specific PapG-Galabiose bond

Additional Galabiose blocking experiments showed, that a specific PapG-Galabiose complex preferably opens at forces of 27 and 49 ± 3 pN. The probability for bond opening at 27 pN is naturally enlarged due to the long time of loading at the first plateau under the influence of the thermal noise. But 72% of the bonds withstand forces stronger than the first plateau. This maintains unstacking of the pilus and with it a prolongation of the bonds' lifetime. The second plateau shows a soft increase in force from 50 to 70 pN. This allows the Galabiose bond to rupture at reduced loading rates even if the separation velocity is high. The whole mechanism seems evolutionarily reasonable, because the pilus uses its stretching and restacking properties to stabilize the Galabiose bond but it opens before irreversible disintegration (compare tether formation in human cells (Sun et al. 2005)). The results are in good agreement to previously reported unbinding forces for type IV pili (Merz et al. 2000; Touhami et al. 2006). They are comparable to forces which affect the elongation and retraction of type IV pili and to unstacking forces of type I pili (Maier et al. 2004; Miller et al. 2006). The Monte Carlo simulation of the specific bond provides reasonable values for the natural dissociation rate $K_{Off} = 8.0 \cdot 10^{-4} \pm 5.0 \cdot 10^{-4}$ s^{-1} and the potential width $\Delta x = 0.7 \pm 0.15$ nm. The simulation used presents an effective method to analyze the measured data obtained by probing specific bonds with a single retract velocity. The data are comparable to other single receptor ligand systems (Florin et al. 1994; Neuert et al. 2006). Further studies can reveal, if the PapG-Galabiose bond is comparable to the allosteric catch-bond mechanism of FimH adhesins, which bind to mannosylated surfaces found by (Thomas et al. 2006). The unstacking-mechanism equally spreads the overall binding force to each pilus and therewith stabilizes the total binding process. The restacking process is slow and the hysteresis, delays restacking even more after an elongation into the regime to open the PapG-Galabiose bond. This might enhance the probability of fishing another Galabiose molecule while reeling in the pilus. This first examination of P-pili stretching and restacking with the AFM gives insights into the mechanisms that sum up the profit of the pili concept.

Acknowledgments This work was supported by the Deutsche Forschungsgemeinschaft, the Alexander von Humboldt Foundation and the Deutscher Akademischer Austauschdienst (DAAD). Technical support from Asylum Research Inc. (Santa Barbara, CA., USA) and helpful discussions with Julia Morfill and Elias Puchner are gratefully acknowledged. Especially, we thank Angelika Kardinal for cell culturing, Susanne Kempter for TEM imaging, Prof. Bernt-Eric Uhlin, Dept. of Molecular Biology, Umeå University, Sweden, for providing the *E. coli* strains and Prof. Ulf J. Nilsson, Organic and Bioorganic Chemistry, Lund University, Sweden, for providing Galabiose and soluble Galabiose.

References

Andersson M, Fallman E, Uhlin BE, Axner O (2006a) A sticky chain model of the elongation and unfolding of Escherichia coli P pili under stress. Biophys J 90:1521–1534

Andersson M, Fallman E, Uhlin BE, Axner O (2006b) Dynamic force spectroscopy of E coli P pili. Biophys J 91:2717–2725

Andersson M, Fallman E, Uhlin BE, Axner O (2006c) Force measuring optical tweezers system for long time measurements of P pili stability. In: Proceedings of SPIE 6088

Benoit M, Holstein T, Gaub HE (1997) Lateral forces in AFM imaging and immobilization of cells and organelles. Eur Biophys J Biophys Lett 26:283–290

Binnig G, Quate CF, Gerber C (1986) Atomic force microscope. Phys Rev Lett 56:930–933

Bippes CA, Humphris ADL, Stark M, Muller D, Janovjak H (2006) Direct measurement of single-molecule visco-elasticity in atomic force microscope force-extension experiments. Eur Biophys J Biophys Lett 35:287–292

Bullitt E, Makowski L (1995) Structural polymorphism of bacterial adhesion pili. Nature 373:164–167

Bullitt E, Makowski L (1998) Bacterial adhesion pili are heterologous assemblies of similar subunits. Biophys J 74:623–632

Bullitt E, Jones CH, Striker R, Soto G, JacobDubuisson F, Pinkner J, Wick MJ, Makowski L, Hultgren SJ (1996) Development of pilus organelle subassemblies in vitro depends on chaperone uncapping of a beta zipper. In: Proceedings of the National Academy of Sciences of the United States of America, vol 93, pp 12890–12895

Evans E, Ritchie K (1997) Dynamic strength of molecular adhesion bonds. Biophys J 72:1541–1555

Evans E, Ritchie K (1999) Strength of a weak bond connecting flexible polymer chains. Biophys J 76:2439–2447

Florin EL, Moy VT, Gaub HE (1994) Adhesion forces between individual ligand-receptor pairs. Science 264:415–417

Friedsam C, Wehle AK, Kuhner F, Gaub HE (2003) Dynamic single-molecule force spectroscopy: bond rupture analysis with variable spacer length. J Phys Condens Matter 15:S1709–S1723

Gill SR, Pop M, DeBoy RT, Eckburg PB, Turnbaugh PJ, Samuel BS, Gordon JI, Relman DA, Fraser-Liggett CM, Nelson KE (2006) Metagenomic analysis of the human distal gut microbiome. Science 312:1355–1359

Grandbois M, Beyer M, Rief M, Clausen-Schaumann H, Gaub HE (1999) How strong is a covalent bond? Science 283:1727–1730

Grandbois M, Dettmann W, Benoit M, Gaub HE (2000) Affinity imaging of red blood cells using an atomic force microscope. J Histochem Cytochem 48:719–724

Jager IL (2001) The ''sticky chain'': a kinetic model for the deformation of biological macromolecules. Biophys J 81:1897–1906

Janovjak HJ, Struckmeier J, Muller DJ (2005) Hydrodynamic effects in fast AFM single-molecule force measurements. Eur Biophys J Biophys Lett 34:91–96

Jass J, Schedin S, Fallman E, Ohlsson J, Nilsson UJ, Uhlin BE, Axner O (2004) Physical properties of Escherichia coli P pili measured by optical tweezers. Biophys J 87:4271–4283

Jiang Z, Mu X, Bullitt E (2002) Site-specific mutations in PapA cause morphologic changes in the structure of P-pili. Mol Biol Cell 13:515A–515A

Larsson A, Ohlsson J, Dodson KW, Hultgren SJ, Nilsson U, Kihlberg J (2003) Quantitative studies of the binding of the class II PapG adhesin from uropathogenic Escherichia coli to oligosaccharides. Bioorg Med Chem 11:2255–2261

Li HB, Oberhauser AF, Fowler SB, Clarke J, Fernandez JM (2000) Atomic force microscopy reveals the mechanical design of a modular protein. In: Proceedings of the National Academy of Sciences of the United States of America, vol 97, pp 6527–6531

Lindberg FP, Lund B, Normark S (1984) Genes of pyelonephritogenic Escherichia-Coli required for digalactoside-specific agglutination of human-cells. Embo J 3:1167–1173

Lugmaier RA, Hugel T, Benoit M, Gaub HE (2005) Phase contrast and DIC illumination for AFM-Hybrids. Ultramicroscopy 104:255–260

Lund B, Lindberg F, Marklund BI, Normark S (1987) The Papg protein Is the Alpha-D-Galactopyranosyl-(1-]4)-Beta-D-Galactopyranose-binding adhesin of Uropathogenic Escherichia-Coli. In: Proceedings of the National Academy of Sciences of the United States of America, vol 84, pp 5898–5902

Maier B, Koomey M, Sheetz MP (2004) A force-dependent switch reverses type IV pilus retraction. In: Proceedings of the National Academy of Sciences of the United States of America, vol 101, pp 10961–10966

Merz AJ, So M, Sheetz MP (2000) Pilus retraction powers bacterial twitching motility. Nature 407:98–102

Miller E, Garcia T, Hultgren S, Oberhauser AF (2006) The mechanical properties of E-coli type 1 pili measured by atomic force microscopy techniques. Biophys J 91:3848–3856

Mu XQ, Bullitt E (2006) Structure and assembly of P-pili: a protruding hinge region used for assembly of a bacterial adhesion filament. In: Proceedings of the National Academy of Sciences of the United States of America, vol 103, pp 9861–9866

Mu XQ, Jiang ZHG, Bullitt E (2005) Localization of a critical interface for helical rod formation of bacterial adhesion P-pili. J Mol Biol 346:13–20

Neuert G, Albrecht C, Pamir E, Gaub HE (2006) Dynamic force spectroscopy of the digoxigenin-antibody complex. Febs Lett 580:505–509

Ohlsson J, Jass J, Uhlin BE, Kihlberg J, Nilsson UJ (2002) Discovery of potent inhibitors of PapG adhesins from uropathogenic Escherichia coli through synthesis and evaluation of galabiose derivatives. Chembiochem 3:772–779

Rief M, Gautel M, Oesterhelt F, Fernandez JM, Gaub HE (1997a) Reversible unfolding of individual titin Ig-domains by AFM. Science 276:1109–1112

Rief M, Oesterhelt F, Heymann B, Gaub HE (1997b) Single molecule force spectroscopy on polysaccharides by AFM. Science 275:1295–1298

Russo TA, Johnson JR (2003) Medical and economic impact of extraintestinal infections due to Escherichia coli: focus on an increasingly important endemic problem. Microbes Infect 5:449–456

Sauer FG, Futterer K, Pinkner JS, Dodson KW, Hultgren SJ, Waksman G (1999) Structural basis of chaperone function and pilus biogenesis. Science 285:1058–1061

Sauer FG, Pinkner JS, Waksman G, Hultgren SJ (2002) Chaperone priming of pilus subunits facilitates a topological transition that drives fiber formation. Cell 111:543–551

Sharma D, Cao Y, Li HB (2006) Engineering proteins with novel mechanical properties by recombination of protein fragments. Angewandte Chemie-International Edition 45:5633–5638

Spinella C, Lombardo S, Priolo F (1998) Crystal grain nucleation in amorphous silicon. J Appl Phys 84:5383–5414

Sun MZ, Graham JS, Hegedus B, Marga F, Zhang Y, Forgacs G, Grandbois M (2005) Multiple membrane tethers probed by atomic force microscopy. Biophys J 89:4320–4329

Thomas WE, Trintchina E, Forero M, Vogel V, Sokurenko EV (2002) Bacterial adhesion to target cells enhanced by shear force. Cell 109:913–923

Thomas W, Forero M, Yakovenko O, Nilsson L, Vicini P, Sokurenko E, Vogel V (2006) Catch-bond model derived from allostery

explains force-activated bacterial adhesion. Biophys J 90:753–764

Touhami A, Jericho MH, Boyd JM, Beveridge TJ (2006) Nanoscale characterization and determination of adhesion forces of Pseudomonas aeruginosa Pili by using atomic force microscopy. J Bacteriol 188:370–377

Vetsch M, Puorger C, Spirig T, Grauschopf U, Weber-Ban EU, Glockshuber R (2004) Pilus chaperones represent a new type of protein-folding catalyst. Nature 431:329–332

Zhang XH, Wojcikiewicz EP, Moy VT (2006) Dynamic adhesion of T lymphocytes to endothelial cells revealed by atomic force microscopy. Exp Biol Med 231:1306–1312